Gating motions in voltage-gated potassium channels revealed by coarse-grained molecular dynamics simulations

Treptow, W.; Marrink, S.J.; Tarek, M.

Published in:
Journal of Physical Chemistry B.

DOI:
10.1021/jp709675e

Publication date:
2008

THE JOURNAL OF PHYSICAL CHEMISTRY B LETTERS

2008, *112,* 3277−3282
Published on Web 02/23/2008

Gating Motions in Voltage-Gated Potassium Channels Revealed by Coarse-Grained Molecular Dynamics Simulations

Werner Treptow,[‡,£,§] Siewert-J Marrink,[†,¶] and Mounir Tarek*[,£]

Center for Molecular Modeling, Department of Chemistry, University of Pennsylvania, 231 South 34th Street, Philadelphia, Pennsylvania 19104-6323, Groningen Biomolecular Sciences and Biotechnology Institute, Department of Biophysical Chemistry, University of Groningen, The Netherlands, and UMR Structure et Réactivité des Systèmes Moléculaires Complexes, Nancy-University, CNRS, France

Received: October 3, 2007; In Final Form: January 17, 2008

Voltage-gated potassium (Kv) channels are ubiquitous transmembrane proteins involved in electric signaling of excitable tissues. A fundamental property of these channels is the ability to open or close in response to changes in the membrane potential. To date, their structure-based activation mechanism remains unclear, and there is a large controversy on how these gates function at the molecular level, in particular, how movements of the voltage sensor domain are coupled to channel gating. So far, all mechanisms proposed for this coupling are based on the crystal structure of the open voltage-gated Kv1.2 channel and structural models of the closed form based on electrophysiology experiments. Here, we use coarse-grain (CG) molecular dynamics simulations that allow conformational changes from the open to the closed form of the channel (embedded in its membrane environment) to be followed. Despite the low specificity of the CG force field, the obtained closed structure satisfies several experimental constraints. The overall results suggest a gating mechanism in which a lateral displacement the S4−S5 linker leads to a closing of the gate. Only a small up−down movement of the S4 helices is noticed. Additionally, the study suggests a peculiar upward motion of the intracellular tetramerization domain of the channel, hence providing a molecular view on how this domain may further regulate conduction in Kv channels.

Introduction

Voltage-gated potassium (Kv) channels constitute one of the two major subfamilies of K^+ channels. These proteins are complex quaternary structures, in which the central hydrophilic pathway for ionic current results from an arrangement of four transmembrane (TM) domains. Each domain contains six helices (S1−S6). S5 and S6 delineate the central pore and are surrounded by segments S1−S4 known as the voltage sensor (VS) domain. The latter senses the variations of the TM voltage and triggers the conformational changes leading to the opening of the channel.[1] Three classes of models have been proposed for the gating of Kv channels, named conventional,[2,3] paddle (based on the crystal structure of the KvAP channel),[4] and transporter.[5] These models disagree, in particular, in the fashion, whereby the VS and the pore domains are coupled.[6]

The so-called conventional model assumes that S4 helices are buried in the protein and slide in a large piston-like motion within their own protein-lined pathway formed by the other voltage sensor segments and the pore domain.[2,3,7] In the transporter model, S4 is also protected from the membrane by the voltage sensor segments. A specific hydration of S4, however, shapes the electric field in the TM domain region. Depolarization of the membrane is believed to produce a rather small TM displacement of S4, which leads to the activation mechanism.[8,9] The paddle model is based on the X-ray structure of KvAP, an archaebacterial channel.[4] In this structure, parts of the S3 segment and S4 are oriented parallel to the membrane−water interface, forming the so-called voltage sensor paddle. It has been proposed that when subject to depolarization, the paddle located near the cytoplasmic face of the membrane in the resting-closed state undergoes a large upward movement.

The KvAP crystal structure has since been shown to disagree with several experimental findings on eukaryotic channels.[10−14] The very recent X-ray data of a Shaker channel (Kv1.2)[15,16] revealed indeed that the KvAP model may not be representative of a native conformation. In the X-ray structure of Kv1.2, S4 adopts a TM orientation, interacting physically with the C terminus of S6 by means of the S4−S5 linker, a small helix connecting S4 and S5. Whereas the displacement of the linker is believed to couple to the closing of the intracellular gate formed by S6,[17] it is not clear whether a large downward movement of the S4−S5 linker, and hence a large TM movement of S4, is a requisite for the gating of the channel.[16,18]

The topology and the conductive properties of the resolved Kv1.2 structure indicate that the channel is open.[19,20] Available structural models of the closed state of a related channel (Shaker family) have been based on modeling strategies to comply with

* To whom correspondence should be addressed. Address: Equipe de dynamique des assemblages membranaires, Unité Mixte de Recherches CNRS UHP 7565, Université Henri-Poincaré, Nancy I BP 239, 54506 Vandoeuvre-lès-Nancy, cedex France. Tel: (33) 3 83 68 40 95. Fax: (33) 3 83 68 43 87. E-mail: mtarek@edam.uhp-nancy.fr.
‡ University of Pennsylvania.
† University of Groningen.
£ Nancy-University.
§ E-mail: treptow@sas.upenn.edu.
¶ E-mail: S.J.Marrink@rug.nl.

10.1021/jp709675e CCC: $40.75

experimental constraints.[13,21−23] Transition from the open to the closed forms so far could only be inferred from the two structures. Here, we use coarse-grain (CG) molecular dynamics simulations of the Kv1.2 channel embedded in a lipid bilayer to study its gating mechanism. The method combines a significant reduction in the number of degrees of freedom with a smoother energy surface[24] compared to that of all-atom models.[25] This approach is, therefore, suitable for investigating microsecond rate processes, as shown by previous CG simulations.[26,27] Recently, such models were used to study the stability of the bacterial KcsA channel and that of the VS domain of the KvAP channel.[28] Here, multiple 0.35 μs simulations of the Kv1.2 channel were performed by considering both the full channel and only the TM domain (Kv1.2^{TM}). Additional control simulations of KvAP were also performed. Overall, our results favor a well-defined gating mechanism involving motions of S4 of the S4−S5 linker that comply with the transporter model.

Methods

The basic parameters for the combined peptide−lipid force field are the same as those used for the lipid force field described previously.[29] It uses a four-to-one mapping, that is, on average, four heavy atoms are represented by a single interaction center. Most amino acids were mapped onto single standard particle types in a similar way as was done recently by other groups.[26−28] Currently, the model considers four main types of interaction sites only: polar (P), nonpolar (N), apolar (C), and charged (Q). For particles of type N and Q, four subtypes (0, d, a, and da) are further distinguished. Subtype 0 applies to groups in which no hydrogen-bonding capabilities exist, d and a are for groups that could act as a hydrogen-bond donor or acceptor, respectively, and da is for groups with both donor and acceptor options. All nonbonded particles interact via a Lennard-Jones (LJ) potential. In addition to the LJ interaction, charged groups (type Q) interact via the normal electrostatic Coulombic potential.

The particle types for most amino acids were estimated from a comparison between simulation results and experimental measurements of the water−oil partitioning coefficients of the amino acid analogues. In the current version of the force field, the experimental values could be reproduced to within 2kT. Details of the assignment of particle types and coarse-grain force field parameters can be found in the Supporting Information (SI) text.

Kv1.2 Channel. CG modeling of Kv1.2 was accomplished as follows. (1) C^{α} and $C^{\beta,\delta,\gamma,\cdots}$ atoms of a full atomistic open-state model of Kv1.2,[30] built on the basis of the solved X-ray crystal structure of the channel,[15] were converted, respectively, into main- and side-chain beads of the CG construct. Details of the construction of the full atomistic model from the X-ray structure, where coordinates for residues in segments S1−S3 were not completely resolved, were reported elsewhere.[30] (2) Except for proline-containing regions, such as the PVP motif of S6, segments in helical conformation were constrained to helices. (3) Main-chain beads along the TM regions were defined as nonpolar (N0 type), whereas those in the water-exposed regions received a polar characteristic (P type) to ensure the correct partitioning of channel segments through the water−lipid environment. (4) No potassium ions were added at the selectivity filter; thus, the channel was modeled at low K^+ concentrations. (5) Finally, in accord with the full atomistic model,[30] the central cavity and cavities in the voltage sensor domain were fully hydrated (viz., ∼181 CG water beads) since these volumes correspond to hydrated regions of the protein with direct implications on the activation-gating process.[5,22,30] The transmembrane domain of the Kv1.2 (Kv1.2^{TM}) model was simply obtained from the coarse-grain Kv1.2 construct after suppression of the T1 domain and the T1−S1 linker. For the KvAP channel, steps 1−4 of the Kv1.2 modeling procedure were reproduced for building the model, considering as a framework the X-ray structure of the channel.[31]

Macromolecular Systems. *Kv1.2 System.* The coarse-grain Kv1.2 channel was inserted at the center of a membrane patch composed of coarse-grained dioleylphosphatidylcholine (DOPC^{CG}) molecules, optimizing the distance between conserved aromatic side chains (belonging to S1 through S3) and the phospholipid head groups. The complete system contained the Kv1.2 channel (viz., 870 beads per subunit), 837 DOPC^{CG} molecules, and 30 517 water^{CG} beads (a total of ca. 45 940 beads). As the channel bears a net charge, counterions were added in the solution to neutralize the overall charge of the simulated system. Forty sodium^{CG} ions (1 sodium^{CG} = +0.7 e) were distributed uniformly in the solvent.

Kv1.2^{TM} System. Here, the Kv1.2^{TM} channel was embedded in the lipid, as described above. The final system was comprised of the channel (viz., 587 beads per subunit), 856 DOPC^{CG} molecules, 12 630 water^{CG} beads, and 12 sodium^{CG} counterions.

KvAP System. The arrangement of the KvAP channel inside of the membrane patch was done by matching the S3−S4 paddle at the intracellular water−lipid interface. The resulting system, containing a total of ∼26 697 beads, was comprised of the channel (viz., 461 beads per subunit), 852 DOPC^{CG} molecules, 12 013 water^{CG} beads, and 18 chloride^{CG} counterions (1 chloride^{CG} = −0.7 e).

CGMD Simulation of K Channels. All simulations were carried out in the flexible NPT ensemble using a modified version of the NAMD program,[32] in which the energy of the valence angles are calculated in the form of a harmonic cosine potential. Nonbonded interactions were cut off at 12 Å using a switching function distance at 10 Å. Pair lists were updated at least once every 10 steps with a pair list cutoff of 12 Å. Long-range electrostatics forces were calculated from the Coulombic potential assuming a relative dielectric constant of $\epsilon = 20$. This value was chosen for explicit screening of charged groups, thus avoiding overestimation of the electrostatic interactions, as in this study, the CG water was a nonpolarizable liquid. Finally, the Berendsen's weak-coupling algorithm was applied to set the pressure (1 atm) and the temperature (300 K) of the system. The 3d periodic boundary conditions were used for all simulations.

Note that the CG model is designed for use close to room or physiological temperatures. The temperature dependence of the model has not been investigated in detail. Standard coupling schemes can be used for both temperature and pressure. The largest feasible integration time step for most systems is δt = 50 fs, but sometimes, a smaller time step is required for stability. Here, the equations of motion were integrated considering a time step of 25−30 fs.

Results and Discussion

Up to five independent CGMD simulations were conducted to relax the Kv1.2 channel embedded in a hydrated DOPC bilayer, spanning over 0.35 μs each. Note that whereas variables (density, length scale, energy, temperature) in the CG model keep their physical meaning, this is not strictly true for the time scale. The effective time sampled, which is reported in this manuscript, is 4 times faster than the actual simulation time, based on a comparison to experimental diffusion rates.[29] This time scale was enough to allow a reorganization of the VS domain that led to a closing of the intracellular gate.

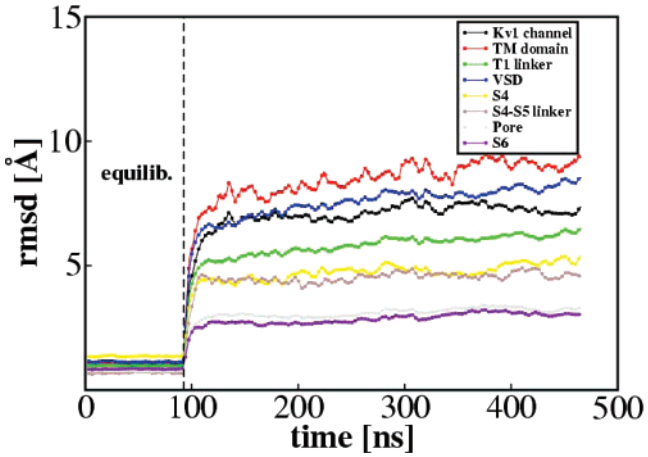

Figure 1. Root-mean-square deviation (rmsd) profiles for the coarse-grain simulation of Kv1.2. Profiles for the whole channel and for the channel's fragments are depicted. The CG structure was constrained during the equilibration stage to allow for full reorganization of the water and lipids. The rmsd's were calculated with respect to the initial coarse grain-structure by superposing the beads of the P helices of the tetramer as the latter did not deviate from the initial construct.

The distance root-mean-square deviations (rmsd) of the Kv1.2 structure from the initial configuration are reported in Figure 1. These indicate that the channel structure has converged during the lapse time of the simulation, with rmsd values varying from 3 Å for the pore domain to ~8 Å for the voltage sensor domain. For comparison, we have performed CGMD simulations of the KscA channel in the membrane environment. Multi-nanosecond all-atom simulations performed by several groups indicate that the KcsA does not deviate significantly from its initial structure. Here, the root-mean-square deviations from the initial structure using the coarse-grain description were ~3 Å at the end of the MD simulations (cf. SI), which indicates that the channel is stable. For comparison, Bond and Sansom report values 3.4 and 1.9 Å for the MscL and KcsA, respectively,[28] values that are comparable to those seen in atomistic MD simulations of membrane proteins.[25] Despite the fact that the coarse graining oversimplifies the real structure of proteins, it, nonetheless, provides a reasonable description of the intramolecular interactions for KcsA in its membrane environment. The results for the KcsA and the Kv1.2 show clearly that the conformational changes in the latter are channel specific. We will demonstrate, in the following, through comparison with experiment, that the final topology of the Kv channel (Figure 2) complies with several structural features.

In the final topology obtained, one may notice, in particular, a tilt of S4 concomitant with a displacement of the S4−S5 linker and a conformational change of the C terminal of S6. Surprisingly, the simulation revealed also an upward motion of the T1 domain and a large movement of the T1−S1 linker.

The conformational changes of the VS segments, as may be probed by the overall mean-square displacements of the latter (cf. Table 1), indicate a downward displacement of S4 of ~3 Å. The main displacement of the S4−S5 linker is sideways (~2 Å) and is coupled to a swivel movement of S6 (Figure 3). The Kv1.2^{TM} construct, in the absence of the T1 domain, underwent similar conformational changes compared to the full-length channel, albeit a higher flexibility was noted for the former. An identical coupling between the VS and the pore was recently inferred from the rosetta modeling of Kv1.2.[23] This method combines homology and de novo modeling guided by experimental constraints derived from structure−function data. Applied to Kv1.2, it favors a model of the closed state that,

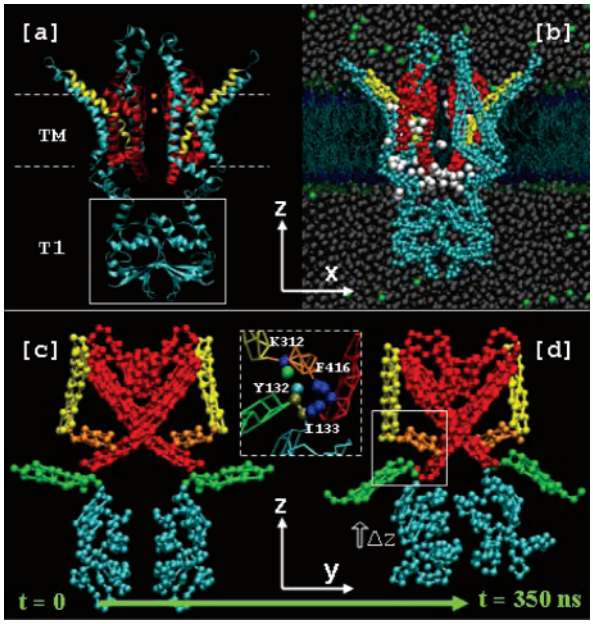

Figure 2. Top: [a] Structure of the Kv1.2 channel highlighting the T1 domain and the transmembrane (TM) domain; the pore helices S5 and S6 are red, the VS segments S1−S3 are cyan, and S4 is yellow. [b] CG representation: The channel is embedded in a DOPC CG−lipid bilayer (licorice) and solvated by CG waters. Beads hydrating the VS and the gate are drawn in white. For clarity, water molecules located in the central cavity are not displayed. Counterions (green) are added to ensure neutrality of the system. Bottom: Topology of the channel at the $t = 0$ [c] and $t = 0.35$ μs simulations [d]. Note the conformational change at the intracellular gate formed by the S6 helices (red) and the upward motion of the T1 domain (cyan). Inset: proximity between the T1−S1 linker (green) and the S4−S5 linker (orange) residues (see text).

TABLE 1: Root-Mean-Square Displacements (rmsd) for the Channel's Fragments[a]

channel		T1	T1−S1 linker	S4	S4−S5 linker	S6
Kv1.2	*xyz*	8.5 ± 1.3	8.2 ± 1.8	4.5 ± 0.9	3.8 ± 0.4	3.8 ± 0.6
	z	6.3 ± 1.7	5.6 ± 0.8	2.5 ± 1.3	1.2 ± 0.4	1.8 ± 0.4
Kv1.2^{TM}	*xyz*			6.1 ± 1.3	5.2 ± 1.6	4.6 ± 1.6
	z			2.8 ± 1.0	1.8 ± 0.4	2.5 ± 0.6
KvAP	*xyz*			4.3 ± 2.6	2.1 ± 0.9	1.0 ± 0.1
	z			1.1 ± 0.2	0.7 ± 0.4	0.5 ± 0.1

[a] The rmsd values (Å) for CG beads of the main chain are estimates of the overall displacement (both in 3 directions, *xyz*, and in one direction, *z* perpendicular to the bilayer plane) of selected segments of the protein (T1 domain, S4 helices,...). These were calculated between the initial conformation of the channel and that obtained at the end of the simulations for each system, and except in the case of the T1 domain, they were averaged over the four monomers. The rmsd values were calculated as $\text{rmsd} = 1/N\sqrt{\sum_{i=1}^{N}(r_i(t)-r_i(0))^2}$ where $\{r_1(t)...r_N(t)\}$ is the set of positions for main-chain beads.

compared to the crystal open structure, indicates a 2−4 Å downward displacement of S4, a clockwise rotation, and a ~35° tilt of its extracellular part with respect to the normal of the membrane surface. The model also predicts that residues of the S4−S5 linker remain in contact with the same residues of the intracellular end of S6 and moves tangentially with respect of the pore domain.

The motion of the S4−S5 linker appears in the present simulations (Figure 3) to be enough to lead to a contraction of the channel around the conserved PVP motif, a region that constitutes the main hydrophobic gate along the conduction pathway.[20,33,34] Figure 4 reports the profile of the pore radius of the Kv1.2 channel.[35] This shows clearly the narrowing of

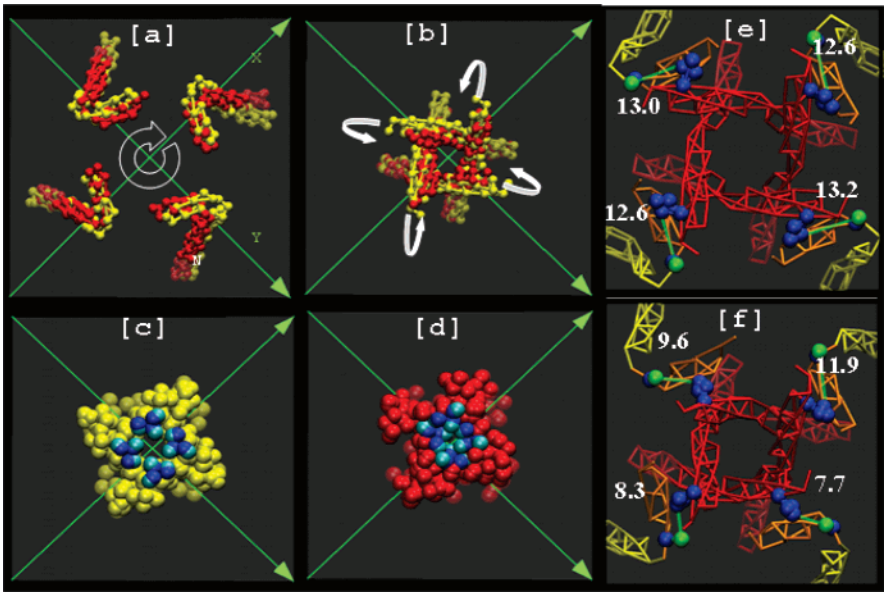

Figure 3. Conformations of S4 and the S4−S5 linker [a] and S6 [b] at the beginning (yellow) and the end (red) of the simulation. Note the counterclockwise swivel motion of S6 (filled white arrows). Narrowing of the Kv1.2 intracellular pore (beads lying within a 15 Å slab located just below the central cavity) occurs between the initial [c] and final [d] steps of the CGMD run. Beads of the PVP motif are drawn in blue and cyan. Distances (Å) between residue K^{312} of the S4−S5 linker (green) and F^{416} of S6 (blue) are reported for the initial [e] and final [f] configurations.

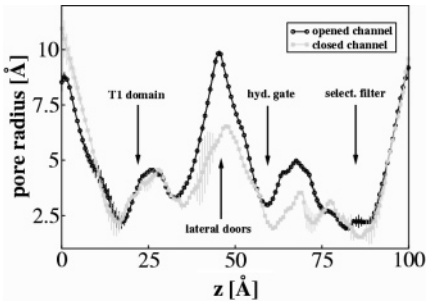

Figure 4. Pore radius profile for the opened and closed conformations of the Kv1.2 channel measured using Hole.[35] Both profiles are averages calculated over a time window of 30 ns at the beginning (black) and at the end (gray) of the simulation. Estimated standard deviations are shown as bars. The profiles span the complete channel, including both the T1 and TM domains. Note that major changes were found for the lateral doors located at the interface between the T1 and TM domains, for the hydrophobic gate formed by the PVPVIV motif in the pore region, and for the central cavity placed between the latter and the selectivity filter.

TABLE 2: Distance Constraints in Kv Channels[a]

			d (Å) from Kv1.2 model	
experiments	state	residue pairs	initial	final
intrasubunit electrostatic interaction	rest	$E^{226}-R^{294}$ (45)	19.2 ± 0.1	17.2 ± 0.5
	p. activ.	$E^{226}-R^{300}$ (46)	8.6 ± 0.2	7.4 ± 3.0
	activ.	$E^{226}-R^{303}$ (46)	8.3 ± 0.2	6.0 ± 1.1
intersubunit disulfide bridge	rest	$S^{289}-E^{350}$ (14)	19.0 ± 0.3	16.2 ± 1.4
		$L^{293}-E^{350}$ (14)	13.6 ± 0.2	12.7 ± 0.7
		$K^{312}-F^{416}$ (37)	12.8 ± 0.3	9.4 ± 1.6
	activ.	$A^{291}-F^{348}$ (11,12)	12.8 ± 0.3	10.5 ± 0.3
		$R^{294}-F^{348}$ (11,13)	10.8 ± 0.5	8.4 ± 2.0
		$R^{294}-A^{351}$ (13)	14.2 ± 0.5	12.6 ± 2.5
intersubunit metal bridge	activ.	$V^{408}-H^{418}$ (34)	9.5 ± 0.4	9.7 ± 2.8

[a] Comparison between probed distances by electrophysiology experiments and results from the MD simulations of the Kv1.2 channel before (initial) and after (final) relaxation of the system. Distances are measured between the geometrical centers of the side-chain beads. Note that the disulfide bridge approach tends to detect distances of ∼15 Å, while formation of metals bridges requires a distance of ∼4.5−6.5 Å between the C^{β} atoms.[47] The rest, activ., and p. activ. states of the channel correspond, respectively, to the closed, open, and intermediate states.

the hydrophilic ionic pathway just above the hydrophobic gate of the channel. Full atomistic modeling of the Kv1.2 channel[20] shows that the constriction at the pore entrance, located near V^{478}, delimits an opening of ∼9 Å diameter and that a mild contraction of this region is enough to preclude ionic transport through the gate. One may, therefore, infer that the clearly witnessed contraction of the intracellular gate (Figures 3 and 4) may be connected to the closing of the channel.

It may be argued here that this is simply a "natural" response of the system given the CG representation, that is, the contraction of the gate that results from transition of the S6 helices from the bend to extended conformation is inherent to the construct. To address this issue, and as a control simulation, we have considered the KvAP structure, for which the gate is also open. The simulations were performed under the same conditions and run over the same time scale. For the KvAP structure, despite a large motion of the VS (cf. SI), the gate remained open. This suggests that contraction at the PVP motif for Kv1.2 is not a simple relaxation of the pore domain (not encountered in the KvAP channel) but may be triggered by the motion of the S4−S5 linker.

The present results corroborate other experimental findings[36] where specific interactions between the S4−S5 linker and S6 appear to stabilize the closed state, participating thus in the coupling of voltage sensing and activation gating. Recently, Ferrer et al.[37] have shown that the linker couples the VS movement to the activation gate. In particular, they identified a specific interaction between D^{540} and L^{666} (located, respectively, in the S4−S5 linker and in S6) in the closed state of the hERG channels. Consistently, we find (Figure 3) that the homologous residues in Kv1.2 (K^{312} and F^{416}) move closer during the simulation.

The final Kv1.2 structure holds several key features as gathered from probed interatomic distances. We report these in Table 2 for residues identified experimentally as being in close proximity at diverse states of the channel. Note that, except for $V^{408}-H^{418}$ and $K^{312}-F^{416}$, all pairs involve either arginines of

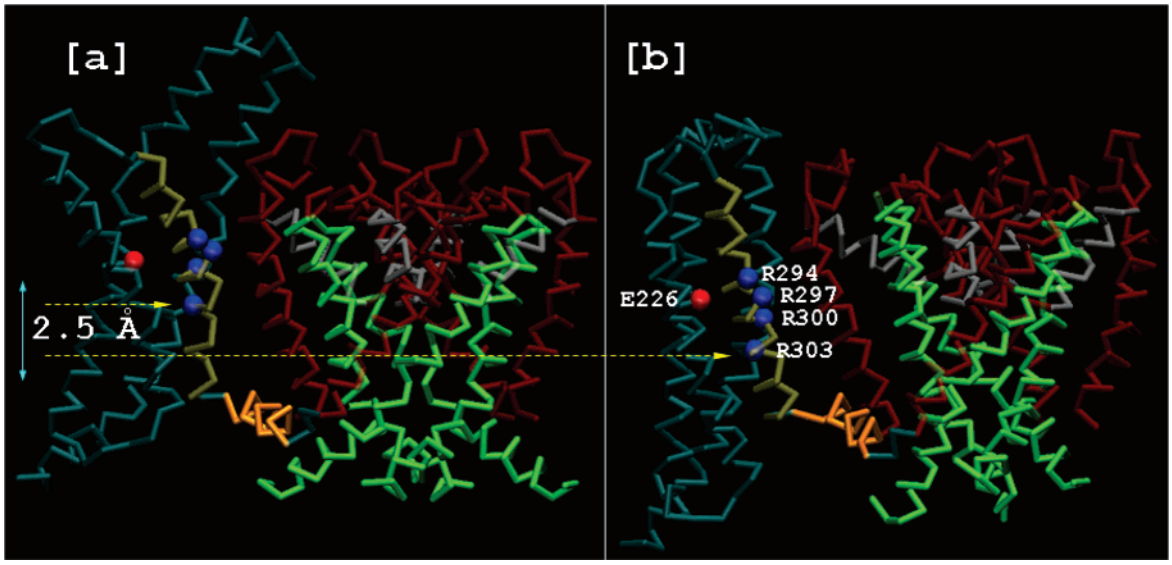

Figure 5. Initial and final configurations of the transmembrane region of the Kv1.2 channel from coarse-grain simulations. The protein is shown as a C^{α} trace, with S6 drawn in green, S5 in red, S4 in gold, and S1−S3 in blue. The P helices joining S5 and S6 are drawn in white, and the S4−S5 linker is in orange. For clarity, the backbone beads of the arginines of S4 are represented by blue spheres. The average displacement of the lower charge (R^{303}) is ∼2.5 Å.

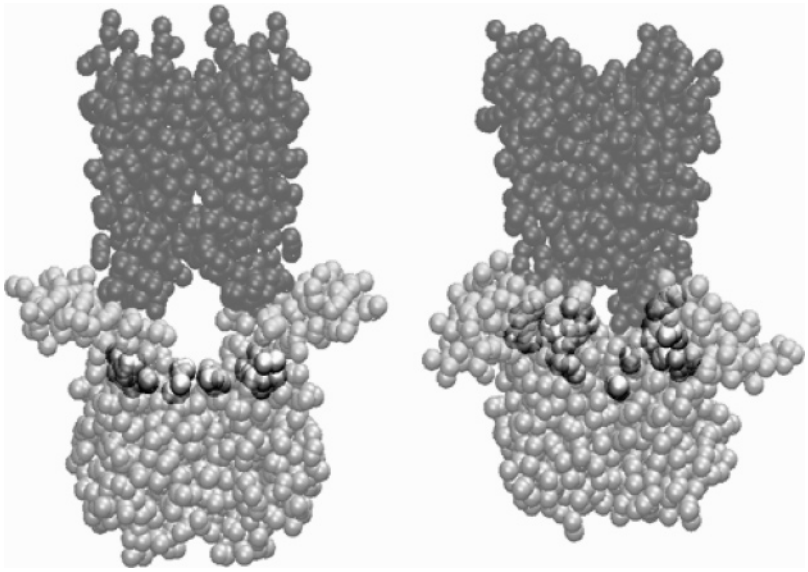

Figure 6. Conformations of the Kv1.2 channel in the open (left) and the closed (right) states, showing the proximity of residues R^{99}, P^{105}, F^{126}, and R^{127} (silver) of the T1 domain (light gray) to the transmembrane domain (dark gray).

S4 or residues located at the top of S4 and, therefore, probe distances between S4 and S5. The local environment near such residues evolves between open and closed states due to a drastic change in hydration.[9,30] EPR measurements on the KvAP channel[38] show that the gating charges in the S4 helix are exposed to the external solution at depolarized potentials. Histidine scanning experiments[9,39] show that for the open channel, the charges are accessible to the solvent from the extracellular side. Upon membrane hyperpolarization, the channel, however, closes, and the charges are no longer accessible from the extracellular but from the intracellular side. Consistent with these experiments, our results show that water is expelled from the top of the VS domain, as the latter undergoes a drastic contraction. Note that while one notices a reduction of the hydration in this region, fine-tuned interactions involving few CG water molecules are not expected to be well reproduced. Given the simplicity of the model and the fact that the mobility of the side chains is not completely accounted for, the state-dependent interatomic distances measured in the model are in rather satisfactory agreement with experiment.

Here, one notes that the "relaxation" of the initial open structure of Kv1.2 in a membrane environment led to a closed conformation at a transmembrane voltage of $\Delta V = 0$ mV. One expects, however, that the channel remains open under this condition. What has then triggered such a conformational change in the CG model? In the CG model, the response of the system to an applied TM voltage is not similar to the case of atomistic simulations[40,41] because the surrounding aqueous solution is not a polar liquid; therefore, the model is somewhat "blind" to an applied voltage. In fact, the physics of the model appears to not favor hydration of the VS domain. Yet, several experiments and simulations have shown that this hydration is required for the channel function.[9,39] Indeed, it has been shown that an increased hydration of S4 is requisite to the activation of the channel.[22] Bell and co-workers have also suggested that S4 lies in extensive water cavities in the open state and that these

crevices collapse upon channel closure, presumably due to a rearrangement of the voltage sensor domain.[10]

The two conformations of the Kv1.2 channel obtained are consistent with this finding, that is, the substantial hydration of the VS domain corresponds to the open initial state, whereas for the closed state, water is expelled from the TM domain. Despite the fact that here the TM voltage conditions are not the driving force for the closing of the channel, the structural modifications and the changes of hydration features accompanying the latter are consistent with the expected transition from the open to closed state. In this transition, only a mild downward displacement of S4 and a lateral displacement of the S4−S5 linker were required (Figure 5). These results, combined with previous full atomistic simulations,[22,30] support the transporter model.

The present study unveiled also a peculiar motion of the intracellular tetramerization T1 domain. The upward motion of the latter favors the interaction between residues of the T1−S1 linker, residues of the S4−S5 linker, and residues in the C terminal of S6 (inset of Figure 2). As a result, external solvent accessibility to R^{99}, P^{105}, F^{126}, and R^{127} (residues of the T1 domain) is reduced due to a contraction of the lateral intracellular portals of the channel at the T1−pore interface (Figure 6). This rationalizes recent measurements showing that the homologous residues H^{104}, C^{110}, C^{131}, and C^{132} in Kv4.1 are protected from MTSET reagents in the closed and inactivated states.[42] It further supports structure−function studies, showing that mutations of polar residues of this domain affect voltage gating in Kv channels.[43,44] It is not clear how much the upward motion of the T1 domain influences the closing of the gate (through contact with S6). This is, however, not the only way such motion may influence the conductive properties of the channel. Indeed, the topology of Kv1.2 indicates that ions gain access to the pore through four "windows" formed by the linker connecting T1 to S1 (the first TM helix). The simulations indicate here that the opening of these passages become smaller as the T1 domain approaches the cytoplasmic membrane face. We anticipate that such a mechanism might further modulate the gating process and directly regulate ion conduction in Kv channels.

Conclusion

Coarse-grained molecular dynamics simulations were used to investigate the gating of the voltage-gated potassium channel Kv1.2 in a membrane environment. From multiple runs, we find that the channel relaxes and closes during the simulation. The coupling between the motions of the VS domain and that of the S6 helix of the gate is ensured mainly by means of lateral displacements of the S4−S5 linkers. This molecular rearrangement necessitates a mild downward translation (∼3 Å) and tilt of S4. The simulations reveal, furthermore, a remarkable upward motion of the tetramerization (T1) domain during the closure of the channel, inducing interactions between the T1−S1 and S4−S5 linkers. Overall, the present results support an activation model in which S4 undergoes a moderate transmembrane displacement and further suggest the role that the T1 domain and T1−S1 linker may play in the gating process.

Acknowledgment. Part of this work was supported by a Centre National de la Recherche Scientifique postdoctoral fellowship to W.T. Calculations were performed at the Centre Informatique National de l'Enseignement Supérieur (Cines).

Supporting Information Available: Details on the force field parameters used, a figure reporting motions of the KvAP channel, and movies of the conformational change of the Kv1.2 channel. Supplementary analyses of the channels' conformations are provided. This information is available free of charge via the Internet at http://pubs.acs.org.

References and Notes

(1) Yellen, G. *Nature* **2002**, *419*, 35.
(2) Larsson, H. P.; Baker, O. S.; Dhillon, D. S.; Isacoff, E. Y. *Neuron* **1996**, *16*, 387.
(3) Horn, R. *Biochemistry* **2000**, *39*, 15653.
(4) Jiang, Y.; Ruta, V.; Chen, J.; Lee, A.; MacKinnon, R. *Nature* **2003**, *423*, 42.
(5) Bezanilla, F. *Trends Biochem. Sci.* **2005**, *30*, 166.
(6) Blaustein, R. O.; Miller, C. *Nature* **2004**, *427*, 499.
(7) Yang, N.; George, A. L. J.; Horn, R. *Neuron* **1996**, *16*, 113.
(8) Bezanilla, F. *Physiol. Rev.* **2000**, *80*, 555.
(9) Starace, D. M.; Bezanilla, F. *Nature* **2004**, *427*, 548.
(10) Bell, D.; Yao, H.; Saenger, R.; Riley, J.; Sielgelbaum, S. *J. Gen. Physiol.* **2004**, *123*, 5.
(11) Broomand, A.; Männikkö, R.; Larsson, P.; Elinder, F. *J. Gen. Physiol.* **2003**, *122*, 741.
(12) Gandhi, C.; Clark, E.; Loots, E.; Pralle, A.; Isacoff, E. *Neuron* **2003**, *40*, 515.
(13) Lainé, M.; Lin, M. A.; Bannister, J. P. A.; Silverman, W. R.; Mock, A. F.; Roux, B.; Papazian, D. M. *Neuron* **2003**, *39*, 467.
(14) Neale, E. J.; Elliott, D. J. S.; Hunter, M.; Sivaprasadarao, A. *J. Biol. Chem.* **2003**, *278*, 29079.
(15) Long, B. S.; Campbell, E. B.; MacKinnon, R. *Science* **2005**, *309*, 897.
(16) Long, S. B.; Campbell, E. B.; MacKinnon, R. *Science* **2005**, *309*, 903.
(17) Lu, Z.; Klem, A. M.; Ramu, Y. *J. Gen. Physiol.* **2002**, *120*, 663.
(18) Ruta, V.; Chen, J.; Mackinnon, R. *Cell* **2005**, *123*, 463.
(19) Khalili-Araghi, F.; Tajkhorshid, E.; Schulten, K. *Biophys. J.* **2006**, *91*, L72.
(20) Treptow, W.; Tarek, M. *Biophys. J.* **2006**, *91*, L26.
(21) Chanda, B.; Asamoah, O. K.; Blunck, R.; Roux, B.; Bezanilla, F. *Nature* **2005**, *436*, 852.
(22) Treptow, W.; Maigret, B.; Chipot, C.; Tarek, M. *Biophys. J.* **2004**, *87*, 2365.
(23) Yarov-Yarovoy, V.; Baker, D.; Catterall, W. A. *Proc. Natl. Acad. Sci. U.S.A.* **2006**, *103*, 7292.
(24) Nielsen, S. O.; Lopez, C. F.; Srinivas, G.; Klein, M. L. *J. Phys.: Condens. Matter* **2004**, *16*, R481.
(25) Ash, W. L.; Zlomislic, M. R.; Oloo, E. O.; Tieleman, D. P. *Biochim. Biophys. Acta* **2004**, *1666*, 158.
(26) Periole, X.; Huber, T.; Marrink, S. J.; Sakmar, T. P. *J. Am. Chem. Soc.* **2007**, *129*, 10126.
(27) Shih, A. Y.; Arkhipov, A.; Freddolino, P. L.; Schulten, K. *J. Phys. Chem. B* **2006**, *110*, 3674.
(28) Bond, P. J.; Sansom, M. S. *Proc. Natl. Acad. Sci. U.S.A.* **2007**, *104*, 2631.
(29) Marrink, S. J.; Vries, A. H.; Mark, A. E. *J. Phys. Chem. B* **2004**, *108*, 750.
(30) Treptow, W.; Tarek, M. *Biophys. J.* **2006**, *90*, L64.
(31) Jiang, Y.; Lee, A.; Chen, J.; Ruta, V.; Cadene, M.; Chait, B. T.; MacKinnon, R. *Nature* **2003**, *423*, 33.
(32) Phillips, J. C.; Braun, R.; Wang, W.; Gumbart, J.; Tajkhorshid, E.; Villa, E.; Chipot, C.; Skeel, R. D.; Kale, L.; Schulten, K. *J. Comput. Chem.* **2005**, *26*, 1781.
(33) Kitaguchi, T.; Sukhareva, M.; Swartz, K. J. *J. Gen. Physiol.* **2004**, *124*, 319.
(34) Webster, S. M.; del Camino, D.; Dekker, J. P.; Yellen, G. *Nature* **2004**, *428*, 864.
(35) Smart, O. S.; Goodfellow, J. M.; Wallace, B. A. *Biophys. J.* **1993**, *72*, 1109.
(36) Decher, N.; Chen, J.; Sanguinetti, M. C. *J. Biol. Chem.* **2004**, *279*, 13859.
(37) Ferrer, T.; Rupp, J.; Piper, D. R.; Tristani-Firouzi, M. *J. Biol. Chem.* **2006**, *281*, 12858.
(38) Cuello, L. G.; Cortes, D. M.; Perozo, E. *Science* **2004**, *306*, 491.
(39) Starace, D. M.; Bezanilla, F. *J. Gen. Physiol.* **2001**, *117*, 469.
(40) Tieleman, D. P. *BMC Biochem.* **2004**, *5*, 10.
(41) Tarek, M. *Biophys. J.* **2005**, *88*, 4045.
(42) Wang, G.; Covarrubias, M. *J. Gen. Physiol.* **2006**, *127*, 391.
(43) Cushman, S. J.; Nanao, M. H.; Jahng, A. W.; deRubeis, D.; Choe, S.; Pfaffinger, P. J. *Nat. Struct. Biol.* **2000**, *7*, 403.
(44) Minor, D. L.; Lin, Y. F.; Mobley, B. C.; Avelar, A.; Jan, Y. N.; Jan, L. Y.; Berger, J. M. *Cell* **2000**, *102*, 657.
(45) Tombola, F.; Pathak, M. M.; Isacoff, E. Y. *Neuron* **2005**, *45*, 379.
(46) Tiwari-Woodruff, S. K.; Schulteis, C. T.; Mock, A. F.; Papazian, D. M. *Biophys. J.* **1997**, *72*, 1489.
(47) Careaga, C. L.; Falke, J. J. *J. Mol. Biol.* **1992**, *226*, 1219.